APPLIED SCIENCES AND ENGINEERING

A tandem radiative/evaporative cooler for weather-insensitive and high-performance daytime passive cooling

Jinlei Li[1]†, Xueyang Wang[1]†, Dong Liang[1]†, Ning Xu[1]†, Bin Zhu[1]*, Wei Li[2], Pengcheng Yao[1], Yi Jiang[1], Xinzhe Min[1], Zhengzong Huang[3], Shining Zhu[1], Shanhui Fan[4]*, Jia Zhu[1]*

Radiative cooling and evaporative cooling with low carbon footprint are regarded as promising passive cooling strategies. However, the intrinsic limits of continuous water supply with complex systems for evaporative cooling, and restricted cooling power as well as the strict requirement of weather conditions for radiative cooling, hinder the scale of their practical applications. Here, we propose a tandem passive cooler composed of bilayer polymer that enables dual-functional passive cooling of radiation and evaporation. Specifically, the high reflectivity to sunlight and mid-infrared emissivity of this polymer film allows excellent radiative cooling performance, and its good atmospheric water harvesting property of underlayer ensures self-supply of water and high evaporative cooling power. Consequently, this tandem passive cooler overcomes the fundamental difficulties of radiative cooling and evaporative cooling and shows the applicability under various conditions of weather/climate. It is expected that this design can expand the practical application domain of passive cooling.

INTRODUCTION

The rapid global industrialization and population boom trigger huge demands for cooling, from buildings, vehicles, electronics, to human beings (*1*–*3*). It also amplifies the energy consumption and related environmental impacts of the traditional vapor compression cooling technique (*1*, *4*, *5*). Therefore, there is an urgent need for developing daytime passive cooling technologies, which are more eco-friendly. To address this need, evaporative cooling has been extensively studied and deployed (*6*, *7*). A cooling power density of ~320 W m^{-2} (at 30°C, calculated in text S1) can be achieved using evaporative cooling based on pure water. The key limitation of standard evaporative cooling is that it demands an external continuous supply of pure water, which not only adds significant complexity to the systems (*8*) but also is seriously limited because of local geographic factors and global water crisis (*9*).

In the past years, as an alternative technique for passive cooling, daytime radiative cooling has also attracted much attention (*10*–*17*). A variety of remarkable subambient daytime radiative cooling designs, such as photonic structures (*11*), hybrid metamaterial films (*18*, *19*), cooling wood (*20*), and polymer structural materials (*21*–*27*), have been demonstrated with cooling power (at ambient temperature) reaching 40 to 110 W m^{-2} on a clear day (*15*, *16*). However, the radiative cooling power is limited to a theoretical value (~150 W m^{-2}). Moreover, the practical radiative cooling performance is heavily dependent on the good weather/climate with a clear sky (*28*).

Here, we propose and demonstrate a tandem radiative/evaporative (TRE) cooling system that seeks to overcome these fundamental difficulties of evaporative and radiative cooling as outlined above. At nighttime, the system uses radiative cooling to assist water harvest from the atmosphere and to store the water in a polymer matrix. At the daytime, the system simultaneously performs both radiative cooling and evaporative cooling under direct sunlight. Unlike conventional evaporative cooling technology, our system creates its own water supply and realizes good cooling performance. In addition, unlike the standard radiative cooling techniques, our system achieves far higher power density and, moreover, can operate effectively over a much wider range of atmospheric conditions. We therefore realize high-performing and weather-insensitive passive cooling even in the scenario where the traditional evaporative or radiative cooling devices cannot work well.

RESULTS

Design principle of the TER cooling system

To discuss our system, we first briefly review some of the basic concepts and limitations of both daytime radiative cooling and evaporative cooling. Daytime radiative cooling requires strong radiative heat dissipation to the cold outer space (3 K) through the atmospheric transparency window (8 to 13 μm), and strong reflection or backscattering of incident sunlight. The heat transfer process also includes incident atmospheric thermal radiation and nonradiative heat exchange due to convection and conduction with ambient. The net cooling power (P_R) therefore can be expressed as

$$P_R = (P_{rad} - P_{amb}) - P_{sun} - P_{conv+cond} \quad (1)$$

in which P_{rad} and P_{amb} denote radiative power from a radiative cooler and absorbed ambient radiation, respectively. P_{sun} is the power of

[1]National Laboratory of Solid State Microstructures, College of Engineering and Applied Sciences, Jiangsu Key Laboratory of Artificial Functional Materials, Collaborative Innovation Center of Advanced Microstructures, Frontiers Science Center for Critical Earth Material Cycling, Nanjing University, Nanjing 210093, P.R. China. [2]GPL Photonics Lab, State Key Laboratory of Applied Optics, Changchun Institute of Optics, Fine Mechanics and Physics, Chinese Academy of Sciences, Changchun 130033, P.R. China. [3]School of Energy Science and Engineering, Central South University, Changsha 410083, P.R. China. [4]Ginzton Laboratory, Department of Electrical Engineering, Stanford University, Stanford, CA 94305, USA.
*Corresponding author. Email: binzhu@nju.edu.cn (B.Z.); shanhui@stanford.edu (S.F.); jiazhu@nju.edu.cn (J.Z.)
†These authors contributed equally to this work.

absorbed sunlight. $P_{conv + cond}$ is the loss of cooling power due to convection and conduction.

Assuming that we maximize the radiative energy out to the outer space and minimize the sunlight input and nonradiative heat exchange, the theoretically maximal cooling power (at ambient temperature) is limited to below 150 W m^{-2} (*28*). Meanwhile, high humidity or cloud can lead to the decrease in or even close of the atmospheric transparency window, therefore resulting in a significant increase in P_{amb} because of the increase in the atmospheric emissivity ε_{amb}, and hence reduction in the cooling power P_R (Fig. 1A, see text S1 for detailed analysis).

Compared with daytime radiative cooling, an evaporative cooling system with pure water can achieve a higher cooling power density of ~320 W m^{-2} (at 30°C, calculated in text S1). However, the complex system designs (for example, water pump, water purification, antifouling, and cooling tower) and high initial cost seriously hinder its wide applications (*29*). Besides, its large and continuous consumption of water is another concern, especially for broad water-stressed regions.

To overcome the limitations of both daytime radiative cooling and evaporative cooling, here we consider a TRE cooling system. The cooling power of such a tandem system can be theoretically calculated as follows

$$P_{TRE} = (P_{rad} - P_{amb}) - P_{sun} - P_{conv+cond} + H_{ev}\dot{m} \quad (2)$$

where H_{ev} is the enthalpy of water evaporation. $\dot{m}$ denotes the evaporation rate of water. In terms of cooling power density, such a tandem system can outperform both standard daytime radiative cooling systems and evaporative cooling systems over a broad range of working temperatures (see Fig. 1B, text S1, and fig. S1 for more details). Assuming an ambient temperature of 30°C as an example, the cooling power of tandem cooling system can reach up to ~470 W m^{-2}, as compared to that of radiative cooling (~150 W m^{-2}) and evaporative cooling (with pure water) system (~320 W m^{-2}).

Here, it is noteworthy that there have emerged a few experimental attempts trying to integrate the advantages of evaporative and radiative cooling in the past year (*30*–*32*). However, so far, superior cooling performance than the single radiative cooling has not been demonstrated. To fully realize the potential of tandem evaporative/radiative cooling systems, there are several fundamental challenges

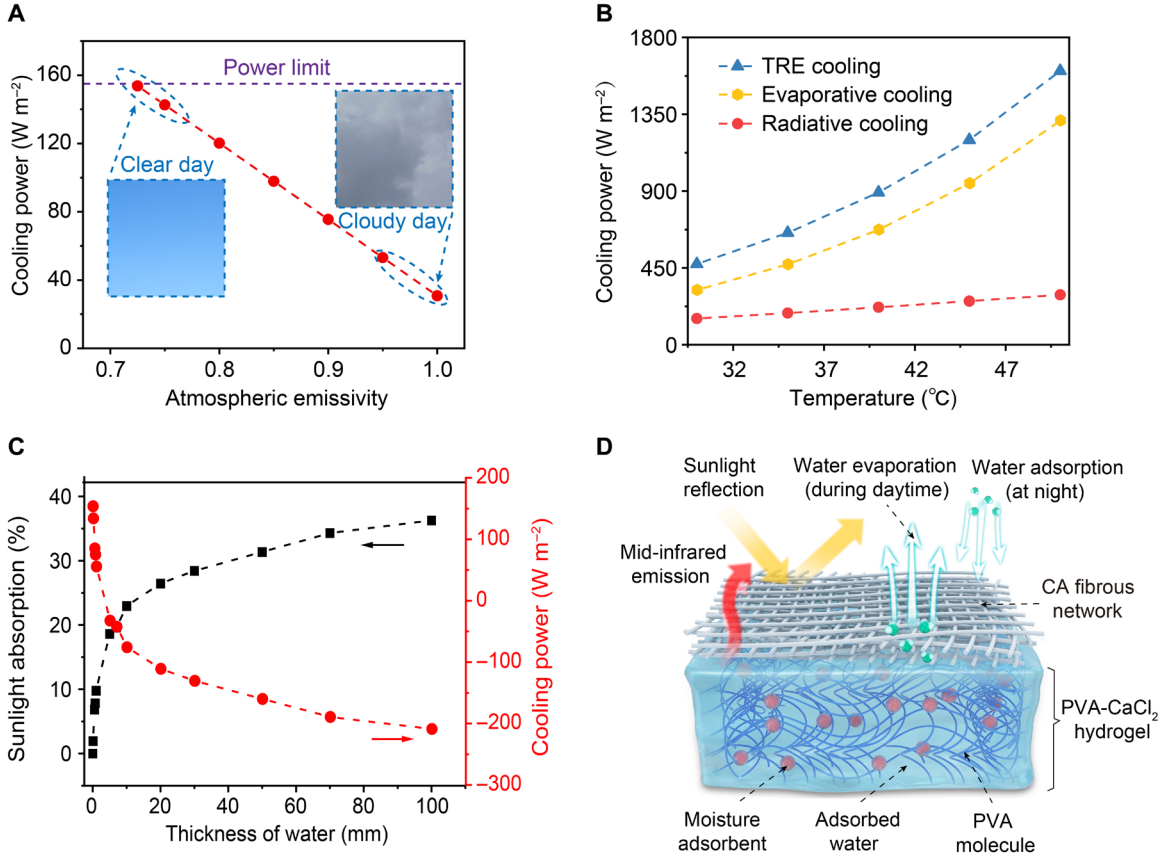

Fig. 1. Comparisons of traditional radiative cooling, evaporative cooling, and the TRE cooling. (**A**) Radiative cooling power (at 30°C) as a function of atmospheric emissivity. The cooling power has a theoretical limit and seriously depends on the atmospheric emissivity, which unavoidably increases with cloud cover and humidity. (**B**) Theoretical cooling power of the TRE cooling, evaporative cooling (from pure water), and radiative cooling. (**C**) Water absorption for sunlight and consequential decline in radiative cooling power (at 30°C). A thin layer of water (several millimeters) will result in a complete disappearance of hard-won radiative cooling power. (**D**) Schematic of the TRE cooling design that consists of the cellulose acetate (CA) fibrous network and poly(vinyl alcohol) (PVA)–$CaCl_2$ hydrogel materials. The CA fibrous network reflects sunlight and radiates energy out. The PVA-$CaCl_2$ hydrogel captures moisture from the ambient during the night and stores the liquefied water for daytime evaporative cooling. Photo credit of (A): N.X., Nanjing University.

that need to be overcome, which were largely neglected in the previous works (*30*–*32*). First of all, water, as is typically used for evaporative cooling, has high absorption of sunlight, especially in the near-infrared (NIR) wavelength (*33*). Such absorption compromises the passive cooling performance. To quantify such an effect, we did a calculation based on the standard AM 1.5G solar spectrum and refractive index distribution of water in (*34*). The result suggests that water with a thickness of only 5 mm will absorb 18.6% power of sunlight, which, if we assume a sunlight intensity of 1 kW m^{-2}, translates to an absorbed power density of 186 W m^{-2} (Fig. 1C). Such absorbed solar power exceeds the maximum theoretical cooling power of a radiative cooler at ambient temperature, severely diminishing the radiative cooling performance. Secondly, the tandem system, including evaporative cooling elements, needs to provide a supply of water. In recent years, there emerge some ingenious materials designs that can realize water self-supply by rain (heavily weather dependent) or moisture harvesting to support evaporative cooling (*35*–*38*), but their cooling performances still have much room for further improvement and should undesirably decline rapidly under strong sunlight as demonstrated below.

Here, we propose a tandem design based on a cellulose acetate (CA) fibrous network atop a poly(vinyl alcohol) (PVA)–$CaCl_2$ hydrogel underlayer (Fig. 1D). The top layer of the CA fibrous network reflects sunlight effectively. Meanwhile, the multiple molecular vibration modes of CA and PVA endow this tandem design with a high mid-infrared emission, especially in the transparency window of the atmosphere. In addition, the underlayer PVA-$CaCl_2$ hydrogel can spontaneously harvest moisture from ambient during the night due to radiative cooling of the structure in the nighttime. The harvested water can then be used for the purpose of evaporative cooling during the daytime. The top porous CA fibrous network with good hydrophobicity does not affect water adsorption/desorption and ensures that the adsorbed water is suppressed beneath the film and only stored in the PVA-$CaCl_2$ hydrogel, avoiding the intrinsic sunlight absorption of water. Therefore, weather-insensitive and high-performance passive cooling can be realized through this tandem design. The atmospheric water capture property of the hydrogel underlayer eliminates the requirement for continuous additional water supply as in traditional evaporative cooling, which not only effectively overcomes the difficulties of mismatched huge cooling demand and limited or even scarce water supply in many places (*9*) but also significantly broadens the sphere of application of such a technique (decoupling the reliance on municipal water, rainwater, or other surface water sources that require pump and collection device).

Material characterizations

We have applied a freeze-drying/electrostatic-spinning synthesis method (see details in Materials and Methods), which has shown potential for scaling up (*39*, *40*), to realize the aforementioned tandem evaporative/radiative cooling design. Figure 2A shows the front (top) and side views (bottom) of the obtained tandem design. The snowy white color of the top CA fibrous network illustrates the effective scattering of visible light, which can be attributed to the structure of randomly stacked nanofibers with a diameter size distribution of around 0.5 to 0.85 μm (Fig. 2B). As corroborated by the calculated scattering efficiency of the CA nanofiber as a function of diameter size across the solar spectrum using the Mie theory (detailed in text S2), such a diameter distribution leads to effective and strong scattering for the wavelength range of 300 to 1000 nm (Fig. 2C) where sunlight has intense spectral emissive power (Fig. 2C). Combining with the high intrinsic emissivity of CA-PVA (details shown below), this design potentially enables good radiative cooling performance under sunlight. Notably, the as-prepared CA fibrous network has good ultraviolet (UV) stability under outdoor exposure as shown in fig. S2, which can be further enhanced via molecular modification (figs. S3 and S4). Such UV stability is highly desirable for practical applications.

The microstructure of the PVA-$CaCl_2$ hydrogel is presented in Fig. 2D. The structure features many micropores with a mean pore diameter of ~1 μm, providing massive pathways for moisture harvest and water evaporation. The moisture adsorption capacities of the PVA-$CaCl_2$ hydrogel reach 0.6, 2.5, 3.5, and 5.1 kg m^{-2} at 40, 60, 80, and 98% relative humidity (tested at 25°C), respectively (Fig. 2E and fig. S5), over 12 hours (during nighttime from 9:00 p.m. to 9:00 a.m.). It is clear that the PVA-$CaCl_2$ hydrogel is more suitable for areas with a relative humidity of >60% at night but has limited capacity for adsorbing sufficient water to sustain the daytime evaporative cooling in the regions with a low relative humidity at night (<55%; see fig. S5). It is expected that by combining the development of atmospheric water capturing materials (*41*–*43*), the applicable humidity range and capacity of moisture adsorption of this TRE design (especially in the areas with a low relative humidity at night) can be further improved, thus providing more water to support daytime evaporative cooling. It is also crucial to evaluate the water evaporation of the PVA-$CaCl_2$ hydrogel under different relative humidities. From Fig. 2F and fig. S6, we find that the mean evaporation rate (in a unit of kg m^{-2} $hour^{-1}$) under a high relative humidity of up to 98% (at 25°C) resembles that under a relative humidity of 40% (only ~25% relatively smaller). The moisture adsorption results clearly ensure that our TRE cooler enables a good evaporative cooling performance under broad ranges of relative humidities/climates.

Given the strong NIR absorption of water, it is crucial to make the CA fibrous network atop hydrophobic and vapor permeable, which can permit penetration of vapor from the ambient and evaporation from underlayer PVA-$CaCl_2$ hydrogel. Thus, the adsorbed water is confined only within the PVA-$CaCl_2$ hydrogel, which minimizes its absorption of sunlight. Therefore, the vapor permeability and hydrophobicity of the CA fibrous network play key roles for the TRE cooler to achieve the excellent dual-functional cooling performance of radiation and evaporation. Figure 2G shows that the water desorption rate of the PVA-$CaCl_2$ hydrogel (0.605 kg m^{-2} $hour^{-1}$) is nearly uninfluenced after being covered with the CA fibrous network (0.599 kg m^{-2} $hour^{-1}$; see Materials and Methods for experimental details), verifying that the CA fibrous network has excellent vapor/moisture transmission, ideal for the evaporative cooling performance of the TRE cooler. In addition, the large water contact angle (131°) of the CA fibrous network (Fig. 2G, inset) confirms its good hydrophobicity, which avoids vapor adsorption of the CA fibrous network, not affecting the radiative cooling performance of the TRE cooler.

As a result, the average reflectivity of the TRE cooler after moisture adsorption in the sunlight wavelength (0.3 to 2.5 μm) still reaches 0.93, similar to that before moisture adsorption (0.95) (Fig. 2H, left axis, before the break). In contrast, the reflectivity of PVA-$CaCl_2$ hydrogel decreases significantly from 0.94 to 0.78 after moisture adsorption (fig. S7), because of the strong absorption of sunlight from water. In addition, the mid-infrared emissive spectrum in Fig. 2H

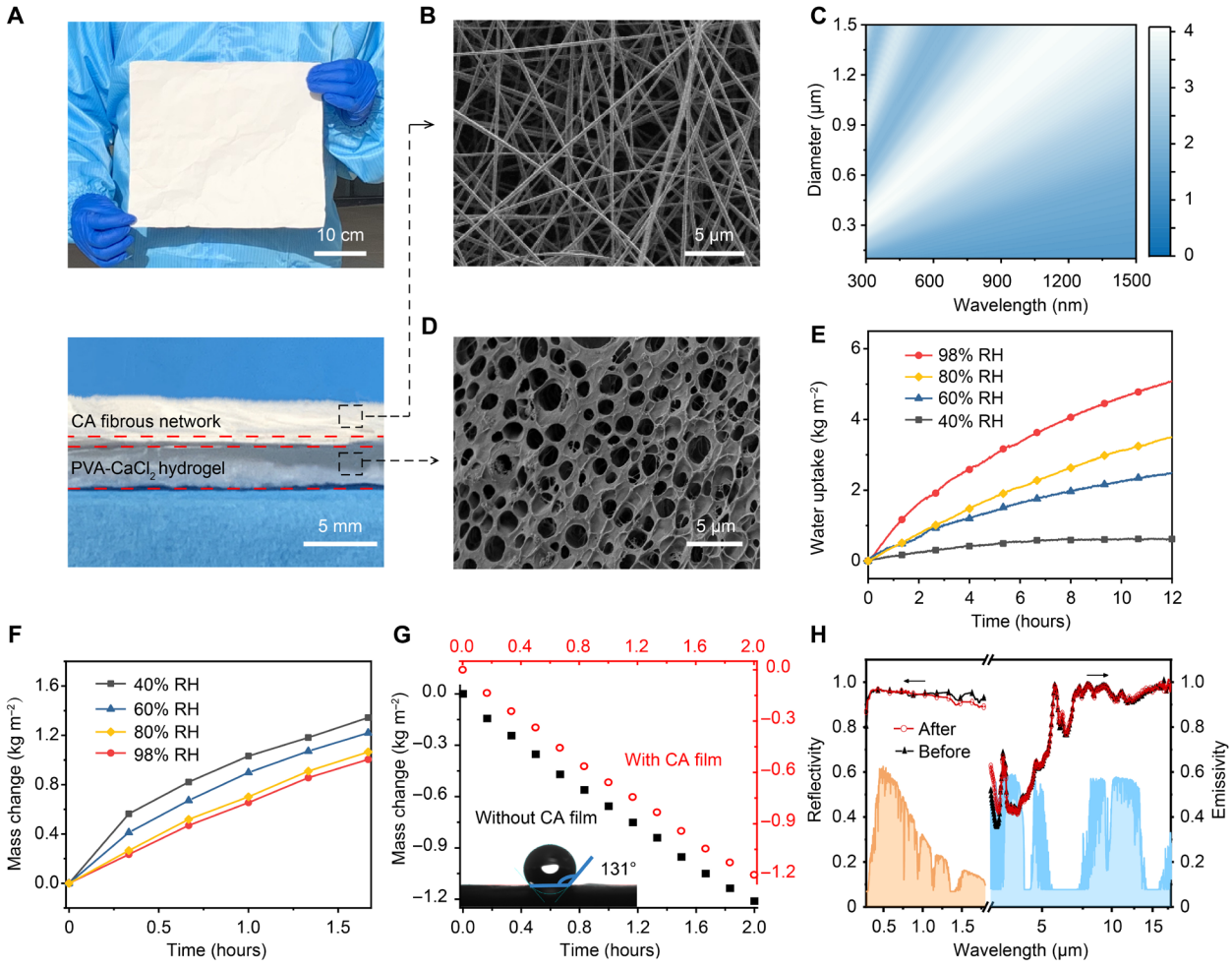

Fig. 2. Characterizations of the TRE cooler. (**A**) Photographs of the front (top) and side (bottom) views for the TRE cooler. (**B**) Scanning electron microscopy (SEM) image of the top CA fibrous network. (**C**) Optical modeling reveals the reflective and scattering effects of the CA fibers. The color bar denotes scattering efficiency (scattering cross section divided by size). (**D**) SEM image of the bottom PVA-$CaCl_2$ hydrogel. The microporous structure provides abundant moisture/vapor paths for moisture capture and water evaporation. (**E** and **F**) Moisture adsorption (at 25°C) and desorption (at 50°C) curves of the PVA-$CaCl_2$ hydrogel over time under varied relative humidities (RH), respectively. (**G**) Water desorption curves of PVA-$CaCl_2$ hydrogel without and with the CA fibrous network. The left right and top bottom axis scales are kept the same. The similar water desorption rates confirm the good moisture/vapor permeability of the CA fibrous network. Inset: Contact angle of 131° for the CA fibrous network, suggesting that it is hydrophobic. (**H**) Sunlight reflectivity (left axis, before the break) and mid-infrared emissivity (right axis, after the break) spectrums of the TRE cooler before and after moisture adsorption. Photo credit of (A): X.W., Nanjing University.

(right, after the break) clearly shows that the TRE cooler is highly emissive in the atmospheric transparent window of 8 to 13 μm (0.94). It is mainly attributed to the multiple vibration modes of CA and PVA molecules of C—OH, C—O, and C—O—C (*20*, *24*). Combining strong sunlight reflectivity, high mid-infrared emissivity, and good atmospheric water harvesting property, this TRE cooler shows its potential for excellent daytime passive cooling performance.

Subambient cooling performance

To experimentally verify the passive cooling performance of the TRE cooler, we performed an outdoor measurement of the temperature via the setups shown in Fig. 3A on both clear and cloudy days (Fig. 3B). Here, a radiative cooler (or a TRE cooler without evaporative cooling function) is set as the control group. In Fig. 3C, we monitored the temperature profiles of the two coolers via thermocouples on a clear day, with a mean sunlight intensity of ~700 W m^{-2} and an averaged ambient temperature of ~35°C (the relative humidity during measurement is shown in fig. S8). Achieving subambient temperature ($T_{Ambient} - T_{Sample}$) is an important indicator to evaluate the cooling performance of a passive cooler. It is observed that the TRE cooler enables a mean subambient cooling temperature of about 10°C, which is 8°C colder than that of the radiative cooler (Fig. 3D).

Besides the excellent subambient cooling performance of the TRE cooler on a clear day, we also measured its cooling performance on a cloudy day. As clouds block the atmospheric window, it is very difficult for the radiative cooler to achieve a subambient cooling effect. As expected, it is found that the temperature of the radiative cooler is ~3.7°C higher than that of the ambient (Fig. 3, E and F). In contrast, the TRE cooler still keeps ~2.7°C below ambient temperature, equivalently 6.4°C below that of the radiative cooler. The results above clearly illustrate that our designed TRE cooler can realize weather-insensitive subambient passive cooling performance.

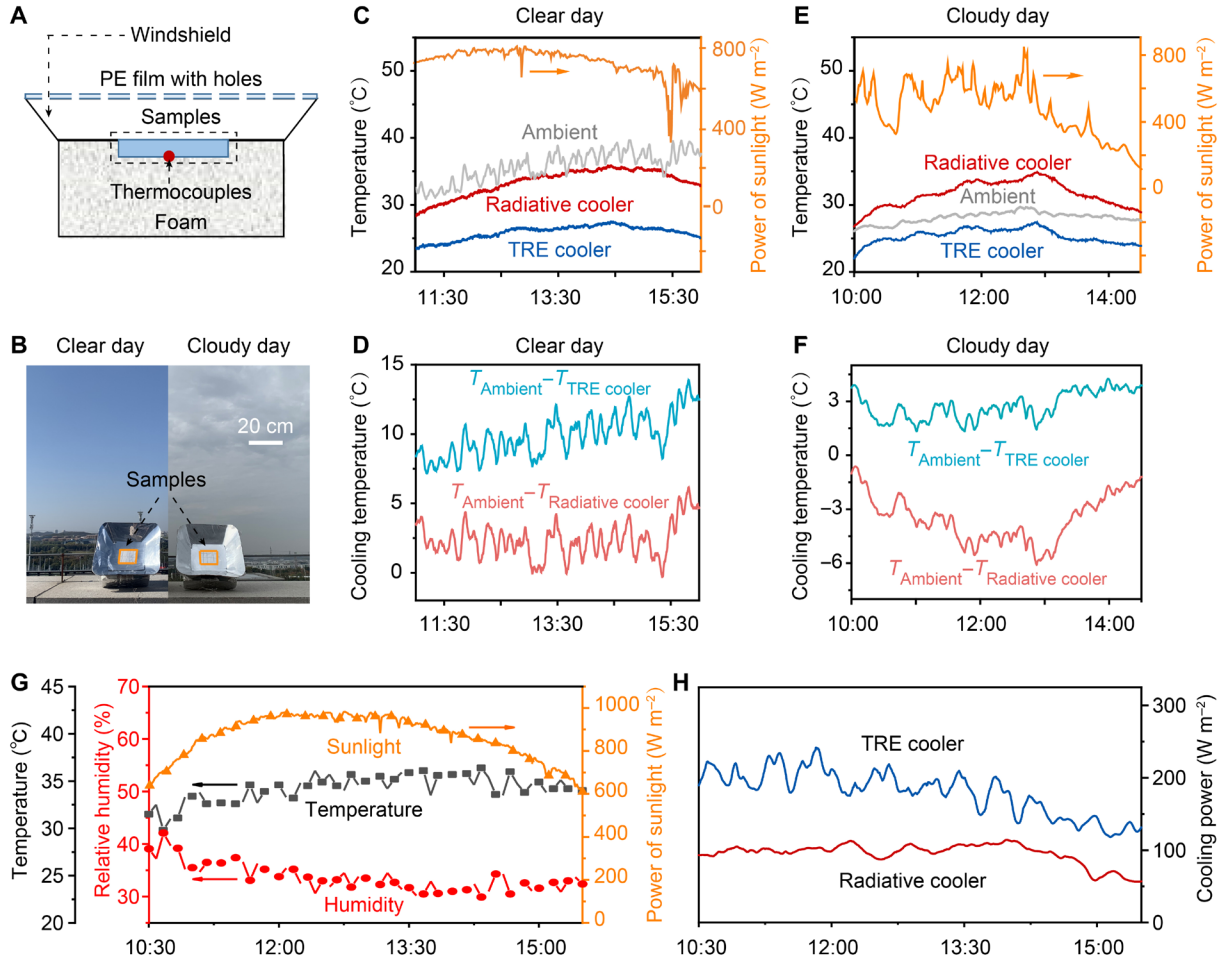

Fig. 3. Subambient cooling performance of the TRE cooler. (**A**) Sectional schematic of the experimental setup used to demonstrate the cooling performance. The polyethylene (PE) film, windshield, and foam are used to minimize the impact of the surroundings. The holes on PE film are designed for vapor escape. (**B**) Cooling performances both on a clear day and a cloudy day are tested. Photographs of the clear (left) and cloudy (right) day during the performance tests. The orange lines highlight samples. (**C** to **F**) Cooling performance during (C and D) a clear day and (E and F) a cloudy day, respectively. (C and E) Environmental conditions (power of sunlight and ambient temperature) and temperature profiles of the two coolers. (D and F) Subambient cooling temperature ($T_{Ambient} - T_{Sample}$) of the two coolers. The TRE cooler exhibits superior cooling performances for both clear and cloudy days, compared to the radiative cooler. (**G**) Ambient conditions of the cooling power test in (**H**). (H) Comparison in cooling power between a TRE cooler and a conventional radiative cooler. Photo credit of (B): D.L., Nanjing University.

We subsequently monitor the cooling power at ambient temperature for both coolers, as it is another common and crucial factor to evaluate/compare the cooling performance. From Fig. 3 (G and H), we find that the cooling power for a conventional radiative cooler (the CA fibrous network, similarly hereinafter) is around 100 W m^{-2}, under a peak sunlight power of ~980 W m^{-2} and at an ambient temperature/relative humidity of ~35°C/33%. This value is consistent with the results reported in most literatures (*17*–*25*). In contrast, the cooling power realized by the TRE cooler (up to 200 to 240 W m^{-2}) is nearly twice as much as that of the radiative cooler and also larger than the power density from evaporative cooling (~100 to 140 W m^{-2}; the power difference between TRE cooler and radiative cooler according to Eq. 2, hereafter the same). It should be noted that the relatively low cooling power enabled by the moisture desorption from the PVA-$CaCl_2$ hydrogel than by evaporation of pure water in Fig. 1B is attributed to the stronger chemical bonding between $CaCl_2$ and water molecule than that between water molecules, which is also consisting with previous findings (*36*, *38*).

Cooling performance at temperatures above ambient

For many practical applications, such as mobile communication stations, vehicles, and condensers of air conditioning, it is often required to cool devices with higher temperatures. Therefore, we also measured the cooling performances of the TRE cooler for a surface with a high temperature of ≥50°C. We adopt test setups that are similar to the one shown in Fig. 3A. What is different is that a Kapton heater with a temperature feedback circuit (namely, the thermostat in Fig. 4A) is introduced beneath the coolers to simulate a hot device with a constant heating load (temperature/power) (*20*, *21*).

The cooling performance of the TRE cooler is also examined under various weather and working conditions. As shown in Fig. 4 (B and C), under a solar power of 725 to 1036 W m^{-2} on a clear day (see fig. S9A for ambient conditions), the TRE cooler at 50°C presents a maximum cooling power of ~700 W m^{-2} and a mean cooling power of ~500 W m^{-2}. In contrast, the cooling power from convectional radiative cooling and evaporative cooling are mere ~200 and ~300 W m^{-2} (corresponding to the previously reported values of stand-alone

evaporative cooling, summarized in table S1), respectively, both much smaller than those of the TRE cooling. Following the cooling power measurement, we monitor the temperature of the two coolers on a clear day with a heating power of ~200 W m^{-2}. As presented in Fig. 4 (D and E), the mean temperatures of the TRE and radiative coolers are ~38° and ~60°C under a solar irradiation of ~850 W m^{-2} (with ambient conditions shown in fig. S9B), respectively. The cooling temperature of the TRE cooler is even ~20°C below that of the conventional radiative cooler.

On a cloudy day, the TRE cooler also exhibits high cooling performance. It is clear from Fig. 4 (F and G) that the cooling power of the radiative cooler at 50°C on a cloudy day with a mean sunlight intensity of ~500 W m^{-2} (the ambient conditions are shown in fig. S9C) is around 200 W m^{-2}, benefiting from the weak sunlight input. In contrast, the TRE cooler still realizes a mean cooling power of ~500 W m^{-2}. It illustrates that the power of evaporative cooling still maintains around 300 W m^{-2}. We also continuously measured the cooling temperature of the two coolers with a heating load of ~200 W m^{-2} over three successive cloudy days (the sunlight power and relative humidity are shown in fig. S10). It is found that the TRE cooler consistently exhibits better cooling performance compared to the radiative cooler (Fig. 4H).

The cooling performance of TRE cooler on a rainy day is also studied. The experimental setup in Fig. 4A can be adapted conveniently to suit the rainy days, as shown in fig. S11. This setup not only protects the TRE cooler from the damage by rains but also enables it to perform cooling even on rainy days. It is found that the TRE cooler realizes ~6.5°C temperature reduction compared with the radiative cooler. Besides, we also compare the cooling performance of the TRE cooler with a typical and traditional evaporative cooling method (evaporation from a wet white textile without the capability of moisture harvesting), and the cooling capacity of our TRE cooler is more than twice as large as that of the white textile (fig. S12). Even compared with most of the stand-alone evaporative cooling devices (without radiative cooling) based on atmospheric water harvesting reported before (table S1), our designed TRE cooler also shows better cooling performance. This is attributed to our tandem design that can collaboratively exploit the advantages of radiative cooling and evaporative cooling.

Cooling performance in different climates

To examine the universal applicability of our TRE cooler under various markedly different climate conditions, the cooling performances of the TRE and radiative coolers are measured at three different

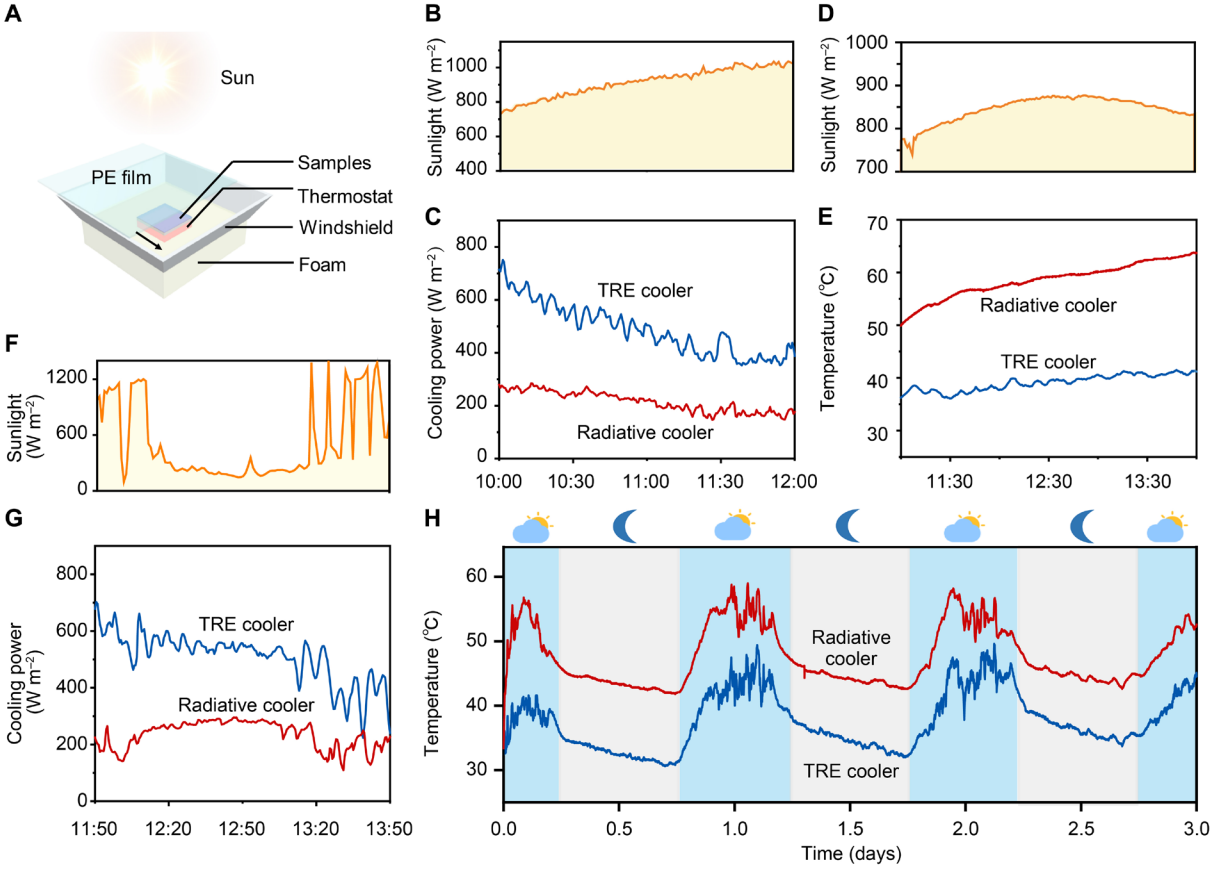

Fig. 4. Cooling performance of the TRE cooler for objects with above-ambient temperature. (**A**) Schematic of the test setup. The thermostat is used to simulate a hot device with a specified heating temperature or power. (**B**) Power of incident sunlight and (**C**) cooling power of the TRE and radiative coolers at 50°C on a clear day. The cooling power of the TRE cooler is more than twice as much as that of the radiative cooler. (**D**) Power of incident sunlight and (**E**) temperature profiles of the TRE and radiative cooler with a heating load of ~200 W m^{-2} on a clear day. The temperature of the TRE cooler is >15°C lower than that of the radiative cooler. (**F**) Power of incident sunlight and (**G**) cooling power of the TRE and radiative coolers at 50°C on a cloudy day. (**H**) Long-term temperature profiles of the TRE and radiative coolers with a heating load of ~200 W m^{-2} on a cloudy day. Blue and gray shaded areas denote cloudy daytime and nighttime, respectively. The TRE cooler performs much better cooling and has excellent cooling stability.

locations over thousands of kilometers apart (see fig. S13) in typical arid, subhumid, and humid climates (Fig. 5, A to C). According to the maps of the climate zone of China and global average yearly humidity, these three climate zones represent the typical global humidity conditions and covers over 70% of the land area on Earth. It is found that the cooling power (Fig. 5, D to F, top) of the TRE cooler is ~100 W m^{-2} larger than that of the radiative cooler and is ~150 W m^{-2} larger than that from evaporative cooling, for all climate types. Our temperature tests (Fig. 5, D to F, bottom) show that the TRE cooler is more than 7°C lower than that of the radiative cooler [the ambient conditions during measurements are presented in Fig. 5 (A to C) in white font and detailed in figs. S14 to S16]. These results consistently suggest that our TRE cooler shows broad applicability under very different climate conditions.

We also present a daylong working of the TRE cooler in the subhumid climate (Fig. 5G). It harvests moisture from 6:00 p.m. to next 10:00 a.m. and performs cooling from 10:00 a.m. to 6:00 p.m. The results show that the PVA-$CaCl_2$ hydrogel adsorbs ~1.28 kg m^{-2} of water, adequately supporting that the TRE cooler continually performs high cooling performance (Fig. 5G and fig. S17 for comparisons in cooling power). Our limited cycling tests in figs. S18 and S19 also prove that such higher cooling performance enabled by the TRE cooler is stable. In the future, we can borrow the design principle of hydrogels in chemical science [see, e.g., (*44*, *45*)] to system study and/or improve the durability of our device to make it robust enough in practical applications.

DISCUSSION

In summary, we demonstrate a tandem passive cooler composed of bilayer polymer materials, simultaneously realizing dual-functional passive cooling of radiation and evaporation. It overcomes the fundamental difficulties of standard evaporative cooling that requires continuous water supply and conventional radiative cooling that

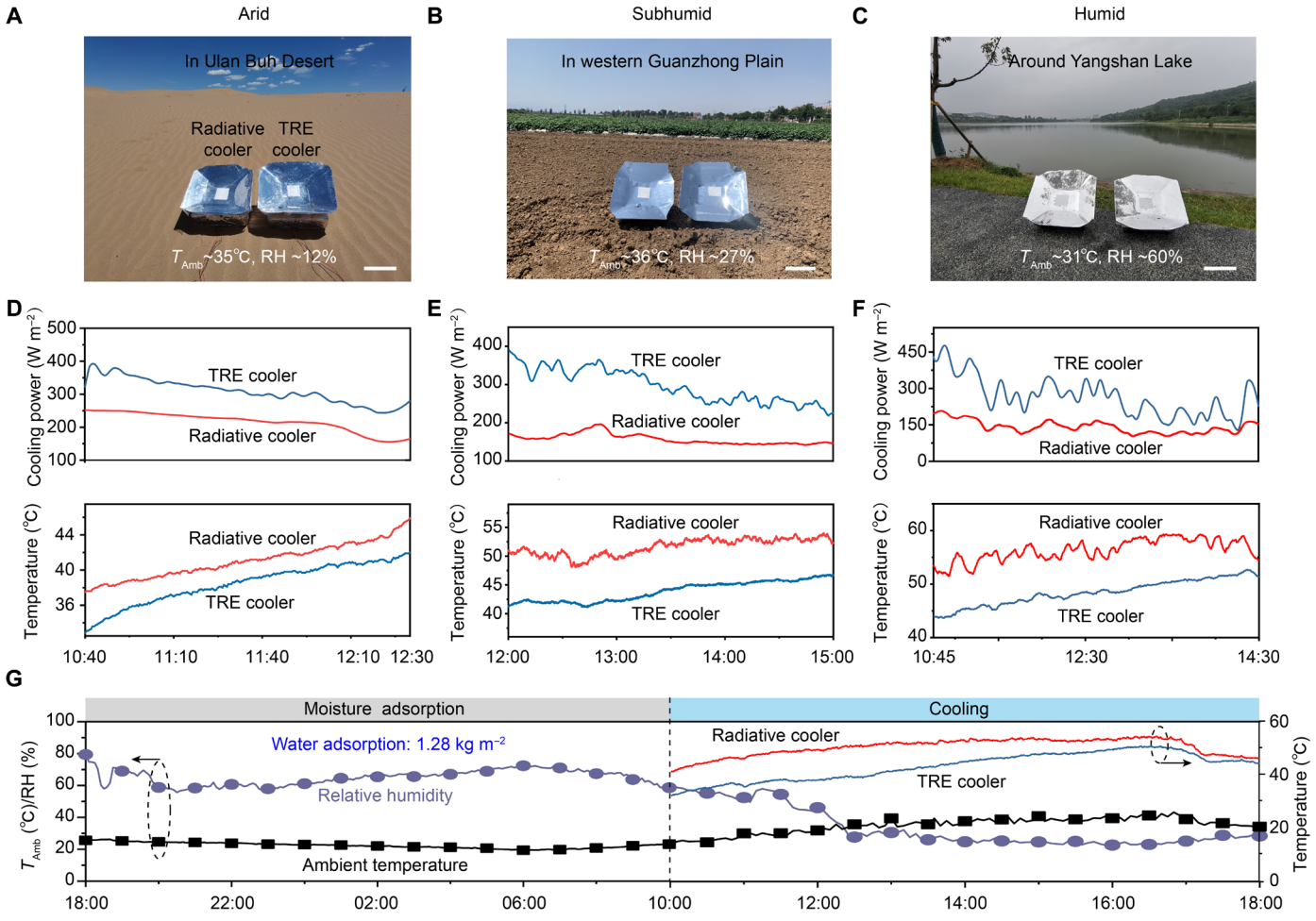

Fig. 5. Cooling performances in different climates. (**A** to **C**) Photographs show the measurements of cooling performances in the (A) arid, (B) subhumid, and (C) humid climates, respectively. The ambient conditions during the cooling performance tests are written in white font. T_{Amb} and RH represent ambient temperature and relative humidity, respectively (hereinafter inclusive). Scale bars, 20 cm. (**D** to **F**) According cooling power (top) and temperature under a thermal load (bottom) in the (D) arid, (E) subhumid, and (F) humid climates, respectively. In all the typical climate types on Earth, the TRE cooler realizes much better cooling performance compared with the radiative cooler. (**G**) Daylong working of the TRE cooler in the subhumid climate. The TRE cooler harvests moisture from 6:00 p.m. to next 10:00 a.m. and performs cooling from 10:00 a.m. to 6:00 p.m. The PVA-$CaCl_2$ hydrogel captures 1.28 kg m^{-2} of water. The temperatures of the two coolers under a thermal load of ~200 W m^{-2} show that the TRE cooler enables continuously better cooling than the conventional radiative cooler throughout the entire period. Photo credit of (A) to (C): J.L. and X.W., Nanjing University.

has limited power density and specific weather/climate requirements. The TRE cooler also outperforms most stand-alone evaporative cooling devices that are designed to harvest atmospheric water to enable self-supply of water in cooling performance and more than doubles the cooling power compared with conventional radiative cooling. Moreover, such a TRE cooler can be versatilely applied over broad scenarios with different weather conditions, climates, and working temperatures. Our calculation shows that there still exists vast potential in improving its cooling performance (fig. S20 and text S1). With more elaborate material and system designs in the future, we expect that this TRE design holds great promise for a broad range of applications, including building, outdoor electronic devices, vehicles, power plants, air conditioning, and so on.

MATERIALS AND METHODS

Preparation of the TRE cooler

The CA fibrous network was fabricated via electrospinning. Acetone and dimethyl formamide were mixed by a volume ratio of 1:4. Then, 17 weight % (wt %) of CA powder was dissolved in the mixture to form a clear solution. The electrospinning was done with a tip-to-collector distance of 15 cm, a voltage difference of ~18 kV, and a mass flow rate of 0.4 ml hour^{-1}. The PVA-$CaCl_2$ hydrogel was prepared by successive processes of gelation, freeze-drying, and loading moisture absorbent. First, PVA was dissolved in deionized (DI) water with a mass ratio of 1:9 at 98°C. Then, alumina nanoparticles (20 wt % of PVA) were added to the dispersion to increase the mechanical strength of the final hydrogel. Subsequently, glutaraldehyde (1.4% volume of DI water, 50 wt %) and HCl (0.6% volume of DI water, 1.2 M) were added to the solution as an initiator and cross-linking agent, respectively. The PVA gel was frozen at −45°C and then thawed in DI water at a temperature of 25°C. The freezing-thawing process was repeated three times. The PVA hydrogel was then freeze-dried at −45°C. Last, the as-prepared PVA hydrogel was immersed in a $CaCl_2$ aqueous solution (50 wt %) to load the hydrogel with moisture absorbent of $CaCl_2$. The as-prepared CA fibrous network and PVA-$CaCl_2$ hydrogel were assembled together to form the TRE cooler.

Material characterizations of the TRE cooler

The microimages of the CA fibrous network and the PVA-$CaCl_2$ hydrogel were captured by scanning electron microscopy (SEM; MIRA3, TESCAN). The test of moisture adsorption/desorption of the PVA-$CaCl_2$ hydrogel was carried out in a constant temperature and humidity chamber (THP-50, ZHIHE). We refer to the previous work (*26*) to monitor the water desorption curves of the PVA-$CaCl_2$ hydrogel without and with the CA fibrous network, therefore evaluating the moisture/vapor permeability for the CA fibrous network. Figure S21 shows a schematic of the test device. The PVA-$CaCl_2$ hydrogel with/without the CA fibrous network was placed on a Kapton heater with a temperature setpoint of ~50°C (realized by a temperature feedback circuit). The environment condition was controlled to have a temperature of ~25°C and a relative humidity of ~70% via the constant temperature and humidity chamber. The reduced mass of the PVA-$CaCl_2$ hydrogel with/without the CA fibrous network was measured periodically (with a time interval of ~10 min) and was divided by the area (5×5 cm^2) of the PVA-$CaCl_2$ hydrogel to obtain the desorption curves. A UV-visible NIR spectrophotometer (UV-360, SHIMADZU) equipped with an integrating sphere (ISR-310) was used to measure the sunlight reflectivity spectrum of samples. The mid-infrared emissivity spectrum was measured with a Fourier transform infrared spectrophotometer (Nicolet iS50R, Thermo Fisher Scientific) equipped with an integrating sphere (4P-GPS-020-SL, Pike).

Cooling performance test

The heating load, a constant temperature or power, was applied by a Kapton heater with a temperature feedback circuit. The cooling temperature was monitored by K-type thermocouples. The heating loads for the temperature tests in the arid, subhumid, and humid climates are controlled to be ~130, ~200, and ~200 W m^{-2}, respectively. The cooling power was obtained by monitoring the heating power of the Kapton heater by a power meter (66205, Chroma), a mature method repeatedly used in literatures (*18*, *20*, *21*). The sunlight power was measured by a solar radiation meter (TBQ) or a portable solar power meter (1333R, TES). The thermocouples used for testing the ambient temperature were placed beneath the polyethylene film. The ambient relative humidity was monitored by a temperature and humidity recorder in a shelter (Tuolaisi Co. Ltd.) or a portable device (COS-03-5, Shandong Renke Control Technology Co. Ltd.). The test sites of cooling power for Figs. 3H and 5E, Figs. 4, (C and G) and 5F, and Fig. 5D are western Guanzhong Plain (in Shaanxi Province, China), Nanjing (in Jiangsu Province, China), and Ulan Buh Desert (in Inner Mongolia, China), respectively. The TRE cooler underwent a whole night of moisture adsorption before performing the daytime cooling. The relative humidities of the ambient during moisture adsorption are ~98% for Figs. 3 and 4 and are shown in figs. S14 to 16 for Fig. 5.

SUPPLEMENTARY MATERIALS

Supplementary material for this article is available at https://science.org/doi/10.1126/sciadv.abq0411

REFERENCES AND NOTES

1. International Energy Agency, "The future of cooling: Opportunities for energy-efficient air conditioning" (International Energy Agency, 2018); www.iea.org/reports/the-future-of-cooling.
2. A. S. Fleischer, Cooling our insatiable demand for data. *Science* **370**, 783–784 (2020).
3. E. Pennisi, Living with heat. *Science* **370**, 778–781 (2020).
4. M. Santamouris, J. J. B. Feng, Recent progress in daytime radiative cooling: Is it the air conditioner of the future? *Buildings* **8**, 168 (2018).
5. M. O. McLinden, C. J. Seeton, A. Pearson, New refrigerants and system configurations for vapor-compression refrigeration. *Science* **370**, 791–796 (2020).
6. A. Pacak, W. Worek, Review of dew point evaporative cooling technology for air conditioning applications. *Appl. Sci.* **11**, 934 (2021).
7. Y. Yang, G. Cui, C. Q. Lan, Developments in evaporative cooling and enhanced evaporative cooling - A review. *Renew. Sustain. Energy Rev.* **113**, 109230 (2019).
8. American Society of Heating, Refrigerating and Air-conditioning Engineers, "*2016 ASHRAE Handbook—HVAC Systems and Equipment*" (American Society of Heating, Refrigerating and Air-Conditioning Engineers, 2016); http://arco-hvac.ir/wp-content/uploads/2016/11/ASHRAE-Handbook-2016-HVAC-Systems-and-EquipmentIP.pdf
9. M. M. Mekonnen, A. Y. Hoekstra, Four billion people facing severe water scarcity. *Sci. Adv.* **2**, e1500323 (2016).
10. E. Rephaeli, A. Raman, S. Fan, Ultrabroadband photonic structures to achieve high-performance daytime radiative cooling. *Nano Lett.* **13**, 1457–1461 (2013).
11. A. P. Raman, M. A. Anoma, L. Zhu, Passive radiative cooling below ambient air temperature under direct sunlight. *Nature* **515**, 540–544 (2014).
12. N. N. Shi, C. Tsai, F. Camino, G. D. Bernard, N. Yu, R. Wehner, Keeping cool: Enhanced optical reflection and radiative heat dissipation in Saharan silver ants. *Science* **349**, 298–301 (2015).
13. E. A. Goldstein, A. P. Raman, S. Fan, Sub-ambient non-evaporative fluid cooling with the sky. *Nat. Energy* **2**, 17143 (2017).
14. B. Zhao, M. K. Hu, X. Z. Ao, N. Chen, G. Pei, Radiative cooling: A review of fundamentals, materials, applications, and prospects. *Appl. Energy* **236**, 489–513 (2019).

15. M. Zeyghami, D. Y. Goswami, E. Stefanakos, A review of clear sky radiative cooling developments and applications in renewable power systems and passive building cooling. *Sol. Energy Mater. Sol. Cells.* **178**, 115–128 (2018).
16. Z. Li, Q. Chen, Y. Song, B. Zhu, J. Zhu, Fundamentals, materials, and applications for daytime radiative cooling. *Adv. Mater. Technol.* **5**, 1901007 (2020).
17. X. Yin, R. Yang, G. Tan, S. Fan, Terrestrial radiative cooling: Using the cold universe as a renewable and sustainable energy source. *Science* **370**, 786–791 (2020).
18. Y. Zhai, Y. Ma, S. N. David, D. Zhao, R. Lou, G. Tan, R. Yang, X. Yin, Scalable-manufactured randomized glass-polymer hybrid metamaterial for daytime radiative cooling. *Science* **355**, 1062–1066 (2017).
19. S. Zeng, S. Pian, M. Su, Z. Wang, M. Wu, X. Liu, M. Chen, Y. Xiang, J. Wu, M. Zhang, Q. Cen, Y. Tang, X. Zhou, Z. Huang, R. Wang, A. Tunuhe, X. Sun, Z. Xia, M. Tian, M. Chen, X. Ma, L. Yang, J. Zhou, H. Zhou, Q. Yang, X. Li, Y. Ma, G. Tao, Hierarchical-morphology metafabric for scalable passive daytime radiative cooling. *Science* **373**, 692–696 (2021).
20. T. Li, Y. Zhai, S. He, W. Gan, Z. Wei, M. Heidarinejad, D. Dalgo, R. Mi, X. Zhao, J. Song, J. Dai, C. Chen, A. Aili, A. Vellore, A. Martini, R. Yang, J. Srebric, X. Yin, L. Hu, A radiative cooling structural material. *Science* **364**, 760–763 (2019).
21. J. Mandal, Y. Fu, A. C. Overvig, M. Jia, K. Sun, N. N. Shi, H. Zhou, X. Xiao, N. Yu, Y. Yang, Hierarchically porous polymer coatings for highly efficient passive daytime radiative cooling. *Science* **362**, 315–319 (2018).
22. A. Leroy, B. Bhatia, C. C. Kelsall, A. Castillejo-Cuberos, M. D. C. H., L. Zhao, L. Zhang, A. M. Guzman, E. N. Wang, High-performance subambient radiative cooling enabled by optically selective and thermally insulating polyethylene aerogel. *Sci. Adv.* **5**, eaat9480 (2019).
23. T. Wang, Y. Wu, L. Shi, X. Hu, M. Chen, L. Wu, A structural polymer for highly efficient all-day passive radiative cooling. *Nat. Commun.* **12**, 365 (2021).
24. D. Li, X. Liu, W. Li, Z. Lin, B. Zhu, Z. Li, J. Li, B. Li, S. Fan, J. Xie, J. Zhu, Scalable and hierarchically designed polymer film as a selective thermal emitter for high-performance all-day radiative cooling. *Nat. Nanotechnol.* **16**, 153–158 (2021).
25. L. Zhou, H. Song, J. Liang, M. Singer, M. Zhou, E. Stegenburgs, N. Zhang, C. Xu, T. Ng, Z. Yu, B. Ooi, Q. Gan, A polydimethylsiloxane-coated metal structure for all-day radiative cooling. *Nat. Sustain.* **2**, 718–724 (2019).
26. P. Hsu, A. Y. Song, P. B. Catrysse, C. Liu, Y. Peng, J. Xie, S. Fan, Y. Cui, Radiative human body cooling by nanoporous polyethylene textile. *Science* **353**, 1019–1023 (2016).
27. H. Zhang, K. C. S. Ly, X. Liu, Z. Chen, M. Yan, Z. Wu, X. Wang, Y. Zheng, H. Zhou, T. Fan, Biologically inspired flexible photonic films for efficient passive radiative cooling. *Proc. Natl. Acad. Sci. U.S.A.* **117**, 14657–14666 (2020).
28. D. Zhao, A. Aili, Y. Zhai, S. Xu, G. Tan, X. Yin, R. Yang, Radiative sky cooling: Fundamental principles, materials, and applications. *Appl. Phy. Rev.* **6**, 021306 (2019).
29. R. Naguib, Total cost of ownership for air cooled and water-cooled chiller systems. *ASHRAE J.* **51**, 42–48 (2009).
30. C. Feng, P. Yang, H. Liu, M. Mao, Y. Liu, T. Xu, J. Fu, T. Cheng, X. Hu, H. Jin Fan, K. Liu, Bilayer porous polymer for efficient passive building cooling. *Nano Energy* **85**, 105971 (2021).
31. Y. Sun, Y. Ji, M. Javed, X. Li, Z. Fan, Y. Wang, Z. Cai, B. Xu, Preparation of passive daytime cooling fabric with the synergistic effect of radiative cooling and evaporative cooling. *Adv. Mater. Technol.* **7**, 2100803 (2021).
32. Z. Xia, L. Li, K. Shi, Z. Fang, X. Fan, Using passive evaporation to improve radiative cooling performance. *J. Photonics Energy* **12**, 012113 (2021).
33. T. A. Cooper, S. H. Zandavi, G. W. Ni, Y. Tsurimaki, Y. Huang, S. V. Boriskina, G. Chen, Contactless steam generation and superheating under one sun illumination. *Nat. Commun.* **9**, 5086 (2018).
34. G. M. Hale, M. R. Querry, Optical constants of water in the 200-nm to 200-μm wavelength region. *Appl. Optics* **12**, 555–563 (1973).
35. A. C. C. Rotzetter, C. M. Schumacher, S. B. Bubenhofer, R. N. Grass, L. C. Gerber, M. Zeltner, W. J. Stark, Thermoresponsive polymer induced sweating surfaces as an efficient way to passively cool buildings. *Adv. Mater.* **24**, 5352–5356 (2012).
36. R. Li, Y. Shi, M. Wu, S. Hong, P. Wang, Photovoltaic panel cooling by atmospheric water sorption-evaporation cycle. *Nat. Sustain.* **3**, 636–643 (2020).
37. C. Wang, L. Hua, H. Yan, B. Li, Y. Tu, R. Wang, A thermal management strategy for electronic devices based on moisture sorption-desorption processes. *Joule* **4**, 435–447 (2020).
38. S. Pu, J. Fu, Y. Liao, L. Ge, Y. Zhou, S. Zhang, S. Zhao, X. Liu, X. Hu, K. Liu, J. Chen, Promoting energy efficiency via a self-adaptive evaporative cooling hydrogel. *Adv. Mater.* **32**, e1907307 (2020).
39. L. Persano, A. Camposeo, C. Tekmen, D. Pisignano, Industrial upscaling of electrospinning and applications of polymer nanofibers: A review. *Macromol. Mater. Eng.* **298**, 504–520 (2013).
40. A. I. Liapis, R. Bruttini, *Handbook of Industrial Drying* (CRC Press, 2020).
41. M. Ejeian, R. Z. Wang, Adsorption-based atmospheric water harvesting. *Joule* **5**, 1678–1703 (2021).
42. F. Fathieh, M. J. Kalmutzki, E. A. Kapustin, P. J. Waller, J. Yang, O. M. Yaghi, Practical water production from desert air. *Sci. Adv.* **4**, eaat3198 (2018).
43. H. Kim, S. R. Rao, E. A. Kapustin, L. Zhao, S. Yang, O. M. Yaghi, E. N. Wang, Adsorption-based atmospheric water harvesting device for arid climates. *Nat. Commun.* **9**, 1191 (2018).
44. J. Sun, X. Zhao, W. R. K. Illeperuma, O. Chaudhuri, K. H. Oh, D. J. Mooney, J. J. Vlassak, Z. Suo, Highly stretchable and tough hydrogels. *Nature* **489**, 133–136 (2012).
45. M. Hua, S. Wu, Y. Ma, Y. Zhao, Z. Chen, I. Frenkel, J. Strzalka, H. Zhou, X. Zhu, X. He, Strong tough hydrogels via the synergy of freeze-casting and salting out. *Nature* **590**, 594–599 (2021).
46. W. Li, S. Fan, Radiative cooling: Harvesting the coldness of the universe. *Opt. Photonics News* **30**, 32–39 (2019).
47. "Water-Heat of Vaporization" (Engineering ToolBox); *www.engineeringtoolbox.com/water-properties-d_1573.html*.
48. "Evaporation from Water Surface" (Engineering ToolBox); *www.engineeringtoolbox.com/evaporation-water-surface-d_690.html*.
49. J. E. Ayuk, A. P. Mathew, K. Oksman, The effect of plasticizer and cellulose nanowhisker content on the dispersion and properties of cellulose acetate butyrate nanocomposites. *J. Appl. Polym. Sci.* **114**, 2723–2730 (2009).
50. R. M. Raouf, Z. A. Wahab, N. A. Ibrahim, Z. A. Talib, B. W. Chieng, Transparent blend of poly (methylmethacrylate)/cellulose acetate butyrate for the protection from ultraviolet. *Polymers* **8**, 128 (2016).
51. R. Hu, B. Huang, Z. Xue, Q. Li, T. Xia, W. Zhang, C. Lu, H. Xu, Synthesis of photocurable cellulose acetate butyrate resin for continuous liquid interface production of three-dimensional objects with excellent mechanical and chemical-resistant properties. *Carbohydr. Polym.* **207**, 609–618 (2019).
52. X. Li, L. Wang, H. Zhang, X. Du, S. Jiang, T. Shen, Y. Zhang, G. Zeng, Seasonal variations in notification of active tuberculosis cases in China, 2005–2012. *PLOS ONE* **8**, e68102 (2013).
53. Average yearly humidity" (University of Wisconsin-madison); https://digitalfilmmaker.net/ruggard-dry-cabinet-dehumidifier/.
54. F. Zhao, X. Zhou, Y. Shi, X. Qian, M. Alexander, X. Zhao, S. Mendez, R. Yang, L. Qu, G. Yu, Highly efficient solar vapour generation via hierarchically nanostructured gels. *Nat. Nanotech.* **13**, 489–495 (2018).
55. F. Ni, P. Xiao, C. Zhang, W. Zhou, D. Liu, S. Kuo, T. Chen, Atmospheric hygroscopic ionogels with dynamically stable cooling interfaces enable a durable thermoelectric performance enhancement. *Adv. Mater.* **33**, 2103937 (2021).
56. S. Pu, Y. Liao, K. Chen, J. Fu, S. Zhang, L. Ge, G. Conta, S. Bouzarif, T. Cheng, X. Hu, K. Liu, J. Chen, Thermogalvanic hydrogel for synchronous evaporative cooling and low-grade heat energy harvesting. *Nano Lett.* **20**, 3791–3797 (2020).
57. P. Yang, C. Feng, Y. Liu, T. Cheng, X. Yang, H. Liu, K. Liu, H. Fan, Thermal self-protection of zinc-ion batteries enabled by smart hygroscopic hydrogel electrolytes. *Adv. Energy Mater.* **10**, 2002898 (2020).

Acknowledgments: We acknowledge intriguing discussion about air conditioning with F. Li from Midea. We acknowledge the microfabrication center of the National Laboratory of Solid State Microstructures (NLSSM) for technical support. J.Z. acknowledges the support from the XPLORER PRIZE. **Funding:** This work is jointly supported by the National Natural Science Foundation of China (nos. 52002168, 52102262, 12022403, 51925204, 11874211, 62134009, 62121005, and 61735008), National Key Research and Development Program of China (nos. 2021YFA1400700 and 2017YFA0205700), Science Foundation of Jiangsu (BK20190311 and BK20200340), Key Science and Technology Innovation Program of Shandong Province (2019JZZY020704), Excellent Research Program of Nanjing University (ZYJH005), and the Fundamental Research Funds for the Central Universities (nos. 021314380184, 021314380214, 021314380208, 021314380190, 021314380140, and 021314380150). S.F. acknowledges the support of the U.S. Department of Energy (grant no. DE-FG-07ER46426). **Author contributions:** J.Z., B.Z., J.L., and N.X. conceived and planned this research. J.L., X.W., D.L., P.Y., Y.J., X.M., and Z.H. did the experiments. W.L. and S.F. contributed to the optical modeling and thermal analysis. J.L., X.W., D.L., N.X., B.Z., W.L., S.F., S.Z., and J.Z. organized the data and wrote the manuscript. All authors discussed the results and approved the final version of the manuscript. **Competing interests:** The authors declare that they have no competing interests. **Data and materials availability:** All data needed to evaluate the conclusions in the paper are present in the paper and/or the Supplementary Materials.

Submitted 14 March 2022
Accepted 30 June 2022
Published 12 August 2022
10.1126/sciadv.abq0411